Preprints (www.preprints.org) | NOT PEER-REVIEWED | Posted: 25 October 2019 doi:10.20944/preprints201910.0284.v1

Peer-reviewed version available at Atmosphere 2020, 11, 114; doi:10.3390/atmos11010114

Article

Analysis of Raindrop Shapes, Fall Velocities, and Scattering Calculations during Tropical Storm Nate

Merhala Thurai[1*], Sophie Steger[2], Franz Teschl[2], Michael Schönhuber[3]

[1] Department of Electrical and Computer Engineering, Colorado State University, Fort Collins, CO 80523, USA; merhala@colostate.edu (M.T.)
[2] Institute of Communication Networks and Satellite Communications, Graz University of Technolog, Austria; sophie.steger@student.tugraz.at (S.S.), franz.teschl@tugraz.at (F.T.)
[3] Joanneum Research, Graz, Austria; michael.schoenhuber@joanneum.at (M.S.)
* Correspondence: merhala@colostate.edu; Tel.: +1-970-491-7678

Abstract: Tropical storm Nate, which was a powerful hurricane prior to landfall along the Alabama coast, traversed north towards our instrumented site in Hunstville, AL. The rain bands lasted 18 h and the 2D-video disdrometer (2DVD) captured the event which was shallow and indicative of pure warm rain processes. Measurements of raindrop size, shape and velocity distributions are quite rare in pure warm rain and are expected to differ from cold rain processes. In particular, asymmetric shapes due to drop oscillations and their impact on polarimetric radar signatures in warm rain have not been studied so far. Recently, the 2DVD data has been used for 3D reconstruction of asymmetric raindrop shapes but their fraction (relative to the more common oblate shapes) in warm rain has yet to be ascertained. Here we compute the scattering matrix drop-by-drop using Computer Simulation Technology integral equation solver for drop sizes>2.5 mm. From the scattering matrix elements, the polarimetric radar observables are simulated by integrating over 1 minute consecutive segments of the event. These simulated values are compared with dual-polarized C-band radar data located at 15 km range from the 2DVD site to evaluate the contribution of the asymmetric drop shapes.

Keywords: raindrop shapes; asymmetric rain drops; scattering calculations; polarimetric radar; 2D-video distrometer

---

1. Introduction

One of the important applications of polarimetric radar is the measurement of rainfall whose accuracy depends critically on the assumed drop shape model which under equilibrium (i.e., balance of aerodynamic, surface tension and gravitational forces) was derived numerically by Beard and Chuang [1]. However, rain drops (with D>0.7 mm or so) do oscillate due to wake instabilities or time-varying drag but the oscillation modes (axisymmetric or asymmetric) and the distribution of oscillation amplitudes are not theoretically predictable. In laminar flow the wind-tunnel experiments of Szakáll et al. [2] showed that larger drops (>2.0 mm) oscillate primarily in the axisymmetric oblate-prolate mode with smaller amplitude asymmetric modes mixed in. These wind-tunnel data (based on high speed camera images of different sized suspended drops over a few seconds) were consistent with the earlier 80 m fall 'artificial rain' experiments of drop shapes imaged as individual 'snap shots' with a 2D-video disdrometer (2DVD) [3], [4], [5]. The consistency was demonstrated by the excellent agreement between time-averaged axis ratios and amplitudes as a function of drop size from the wind-tunnel data with the ensemble-based axis ratio averages and standard deviations from the (80 m fall) 2D-video data and has given confidence in using the average oblate axis ratio versus D relations used in rain rate retrieval algorithms.

A relatively recent advance has been the use of 2DVD in reconstructing the 3D shapes of natural rain drops even if they are asymmetric [6], [7], and further to calculate the scattering matrices of such asymmetric (and the detected symmetric shape) drops using advanced electromagnetic scattering codes [8], [9]. This enables simulation of what is termed 'drop-by-drop' integration to arrive at the radar reflectivity, the differential reflectivity and the copolar correlation coefficient [10]. Comparing the 'drop-by-drop' with the 'bulk' simulations of the same event using the average oblate axis ratio versus D relations enabled a determination of the importance of asymmetric shapes to the rain rate retrieval algorithms as well as the conditions under which asymmetric drop shapes occur more frequently as in one example of an intense line convection [10], [11]. However, in less intense convection or in pure warm rain process (coalescence) dominated events, the frequency of occurrence of asymmetric drops shapes and their impact on rain rate retrieval algorithms is not known. While it is known that small drops dominate the size distributions in tropical rain with active warm rain processes relative to ice dominated deeper convection at the same rain rate, it has been speculated that in the ice dominated cases, asymmetric shapes due to oscillations can be dampened by residual tiny ice cores in the nearly fully melted drops (originating as graupel or tiny hail aloft). On the other hand, pure warm rain processes have no such damping mechanism and thus might exhibit more frequent occurrence of asymmetric shapes. Thus, this article presents 2DVD-based reconstructions of drop shapes in the outer band remnants of tropical storm Nate as it moved across our instrumented site in Huntsville, Alabama. 'Drop-by-drop' scattering simulations are performed and compared with 'bulk' oblate shape assumptions and compared with observations from a scanning C-band radar located 15 km away from the instrument site. Also presented are fall velocities and drop horizontal velocities determined from the 2DVD measurements, specifically for the larger drops (> 2 mm).

The paper is organized as follows. In section 2, we give an overview of tropical storm (TS) Nate and an outline of the specific instruments and measurements pertaining to this study. In section 3, processing of the 2DVD-based images is presented, together with drop horizontal velocities which are obtained as a by-product of the de-skwing procedure of the drop images. Section 4 outlines the scattering calculation procedure and section 5 presents the single particle radar cross-sections calculated for all drops with D > 2.5 mm as well as their differential relectivities. In section 6, the computed reflecitivity and differential reflectivity based on the scattering calculations over a 1-minute interval are compared with the C-band radar measurements over the instrument site, for the entire duration of the Nate event at the instrument site. The main conclusions are summarized in section 7 as well as discussion on each of the main conclusion points.

2. TS Nate Description and Observations in Huntsville

Tropical system Nate originated as a fast moving hurricane which made landfall on the US Gulf Coast. It made its second landfall in the US causing storm surge, flooding buildings, and beach erosion. More inland, Nate weakened to a tropical storm after being embedded within fast mid-latitude westerlies while moving north towards Hunstville, Alabama. The rain bands lasted 18 h over the instrumented site at the University of Alabama, Huntsville (UAH) giving rise to total rain accumulation of over 31 mm. Fig.1 shows the radar mosaic image at 14:45 UTC on 08 October 2017. The rain bands, although noticeable, are not highly defined. The 2DVD [12] captured the event which, at times was shallow, indicative of pure warm rain processes, and at other times somewhat more intense with clear melting layer. The red dot in Fig. 1 (a) marks the location of the instrument; at the specified time, the inner-most rain band was traversing the instrument.

Apart from the 2DVD, there was also another optical array probe specifically for small and tiny drops (called the Meteorological Particle Spectrometer, MPS) [13], a precipitation occurrence sensor system [14], rain gauges, anemometers, and several other ground instruments. Raingauge data showed 1-minute rain rates to be less than 10 mm/hr, and less than 3 mm/h for much of the time. The

Preprints (www.preprints.org) | NOT PEER-REVIEWED | Posted: 25 October 2019 doi:10.20944/preprints201910.0284.v1

Peer-reviewed version available at Atmosphere 2020, 11, 114; doi:10.3390/atmos11010114

temperature at 2-m height was around 73-75 deg F (23-24 deg C) during much of the storm period (02 to 20 hr UTC). A X-band vertically-pointing Doppler radar [15] located a few meters also made observations over the entire storm event, and a C-band dual-polarization radar (ARMOR) [16], [17], located 15 km from UAH had made regular and frequent scans over the site.

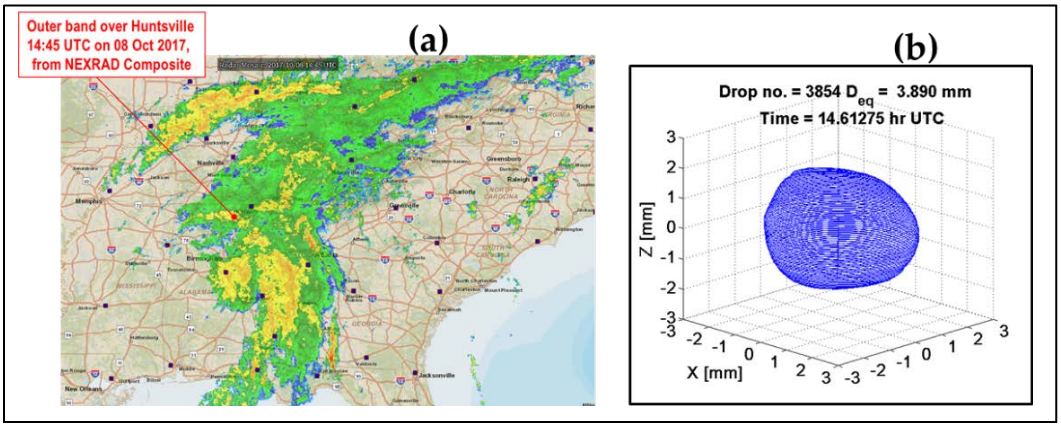

Figure 1. (**a**) Composite (nexrad) radar image of Tropical System Nate over Alabama on 08 Oct 2017 at 14:45 UTC. The location of the 2DVD and other instruments is marked with a red dot; **(b)** Shape of a large drop recorded by the 2DVD at this time (using the 3D reconstruction procedure, see Section 3).

Unlike a previous tropical system, category-1 hurricane Irma which had relatively strong winds and gust conditions associated with it, TS Nate had considerably less wind speeds and turbulence by the time it reached Huntsville. As shown later, the wind speeds were less than 8 m/s (at 10 m height), with no sudden or abrupt change in magnitude nor direction.

3. 2DVD data and processing

The derivation of contoured shapes in two orthogonal planes from 2DVD measurements has been presented in a number of previous publications [18], [19], [4]). Several years later, the contoured shapes in the two orthogonal planes were used to derive the 3-dimensional particle shapes which have been described in [6], [7], and [9]. The procedure involved in the drop contour derivation also includes a 'deskewing' technique which not only yields the corrected contoured shapes for each drop but also its horizontal velocities along the x and y axes, which in turn enables the magnitude and direction to be determined. Along the z-axis, the matching procedure from the 2DVD's two camera images (A and B) enables the fall speeds to be determined on a drop-by-drop basis. However, due to a number of limitations, the velocity and shape information can only be retrieved for relatively large drops, in particular for drops with equi-volume diameter larger than 1.5 or 2 mm. When performing scattering calculations, it is the larger drops which will have the highest contributions to the polarimetric radar variables such as differential reflectivity and copolar correlation coefficient and differential backscatter phase.

The 2DVD measurements during the entire Nate event revealed that the drop diameters (D_{eq}) did not exceed 4 mm. There were 601 drops with $D_{eq} > 2.5$ mm out of 1,467,540 drops in total; out of these, only 79 drops exceeded 3 mm and only 12 drops exceeded 3.5 mm. One of the biggest drops recorded (3.89 mm) is shown in panel (b) of Figure 1, the time of which corresponds nearly to that of the radar mosaic image in panel (a). This was one of the most-intense periods of the storm over UAH, albeit with relatively modest reflectivity of around 40 dBZ. A small degree of shape deformation is visible.

The magnitude and direction of drop horizontal velocities for all drops > 2 mm derived from the 2DVD deskewing procedure are shown as red points in panels (a), and (b) of Fig. 2, respectively. They are compared with the anemometer measurements at 10 m height (black points) from the same location for most of the storm period (02 to 20 hr UTC). Note some 'smoothing' was applied to the

Preprints (www.preprints.org) | NOT PEER-REVIEWED | Posted: 25 October 2019 doi:10.20944/preprints201910.0284.v1

Peer-reviewed version available at Atmosphere 2020, 11, 114; doi:10.3390/atmos11010114

drop horizontal velocities in order to highlight the close agreement with the wind-sensor measurements. As expected, the response of the drops is to assume and acquire the same horizontal velocities as the ambient wind speed and direction. The close agreement, between the green points and the black points, particularly after 06 hr UTC, is also indicative of the accuracy of the shapes of the reconstructed drops.

In panel (c), we show the percentage of deviation of the drop fall velocities from the expected terminal fall speeds of Gunn-Kinzer [20], again for all drops > 2 mm. The 0% line is marked as a dashed blue line. Fluctuations can be observed, which is to be expected, but they appear to be distributed fairly evenly around the 0% line, throughout the event, although at around 15 hr UTC, a few drops show significantly negative percentages (< -30%) which could be due to the well-known response to turbulence. However, majority of the drops have fall velocities within the expected range of their theoretical fall speeds (e.g. [21] for sea level).

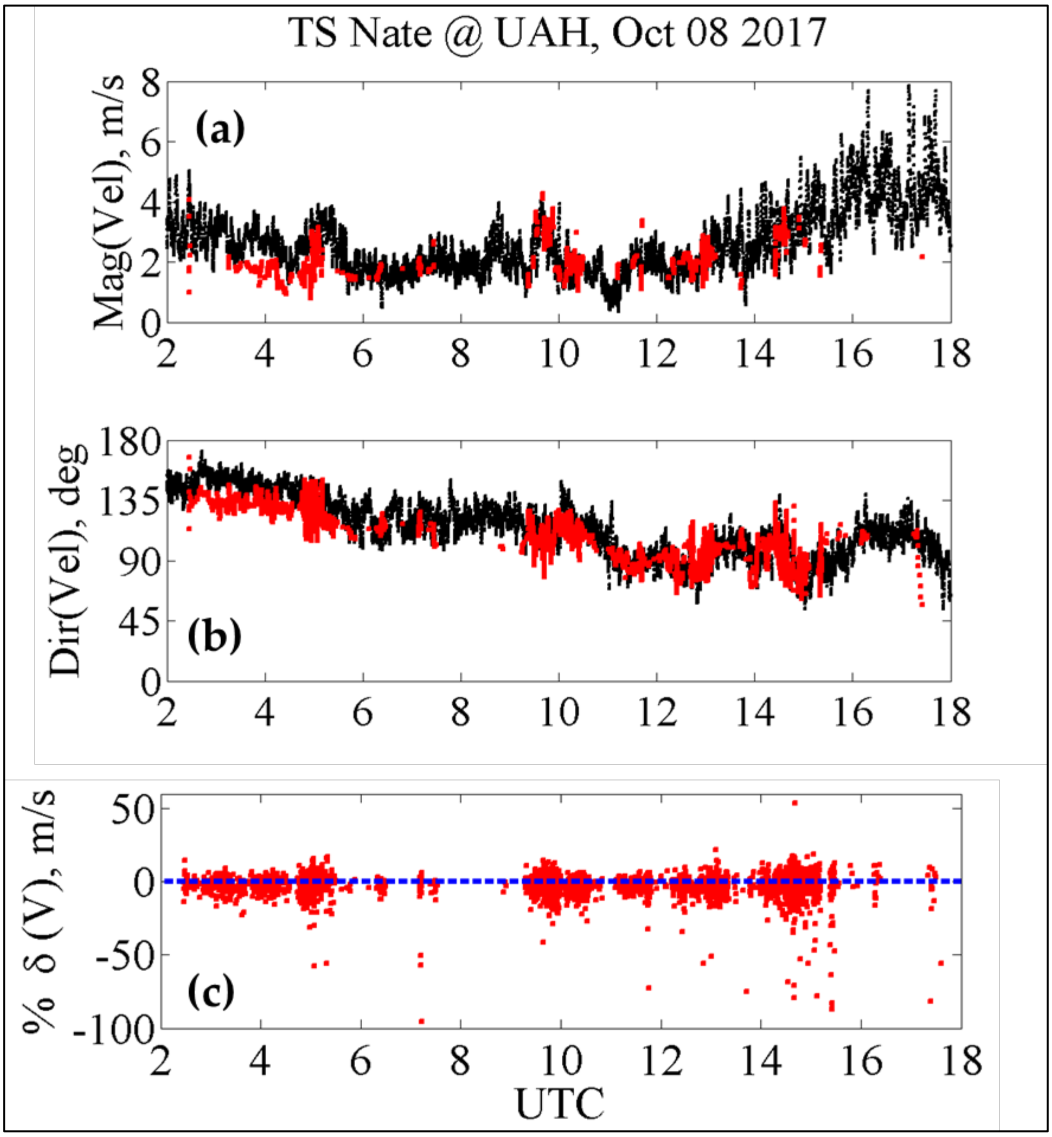

Figure 2. (**a**) and (**b**) Wind speed and wind direction (as black points) from the anemometer at 10 m height at the 2DVD location, respectively, along with the retrieved drop horizontal velocities from the 2DVD in green for all > 2 mm drops; (**c**) percentage change in the drop fall velocities from the 2DVD compared with Gunn-Kinzer equation.

 doi:10.20944/preprints201910.0284.v1

Peer-reviewed version available at Atmosphere 2020, 11, 114; doi:10.3390/atmos11010114

4. Scattering calculations

The scattering calculations have been carried out for all 601 drops captured during the Nate event with D_{eq} > 2.5 mm. The simulation program used within this study is CST Microwave Studio (MWS) of the CST Studio Suite 2019. The use of this software for the scattering calculation of each individual drop has been automated. Visual Basic for Application language was used for creating structures and controlling procedures in CST MWS. In the following paragraphs the main steps of the scattering calculations are outlined.

The 3D shapes of each raindrop was reconstructed with Matlab-software using the procedure described in [6] and [7]. For each drop a STL-file (STL for stereolithography) was generated that characterize the surface geometry of the drop without specifying material or scale information. The STL-files of the drops were imported into CST MWS. For the material, the dielectric properties of water at a temperature of 68 deg F (20 deg C) and a frequency of 5.625 GHz were assumed. Following the model of Ray [22] this leads to a complex permittivity ε of 72.5 - j22.43 (refractive index m = 8.6137 - j1.3020). After importing and scaling the shape, a meshing algorithm is performed by CST MWS. Figure 3(a) shows the mesh of an example drop. The drop is approximated by a set of triangles that are connected by common edges or by corner points. The triangulation is based on the outer surfaces that occur when reconstructing the drop. The 3D reconstruction is carried out with an angular resolution of 10 degrees in azimuth and with 0.05 mm vertical resolution. If a drop e.g. has a height of 3 mm this procedure leads to approximately 36 * (3 / 0.05) = 2160 quadrangular planar surfaces on the outside. As each surface is split in order to form triangles, the number of surfaces duplicates.

Figure 3(b) shows the histogram of the edge length of the triangulation of the drop shown in Figure 3(a). For the given drop the shortest edge length is approx. 0.03 mm and the largest edge length is approx. 0.37 mm. On average the edge length is 0.1 mm. The largest detected drops with an equal volume diameter of ~3.8 mm are approximated by more than 5000 triangles. Given a frequency of 5.626 GHz and therefore a wavelength of 5.3 cm, each drop is modelled with at least 15 grid points per wavelength.

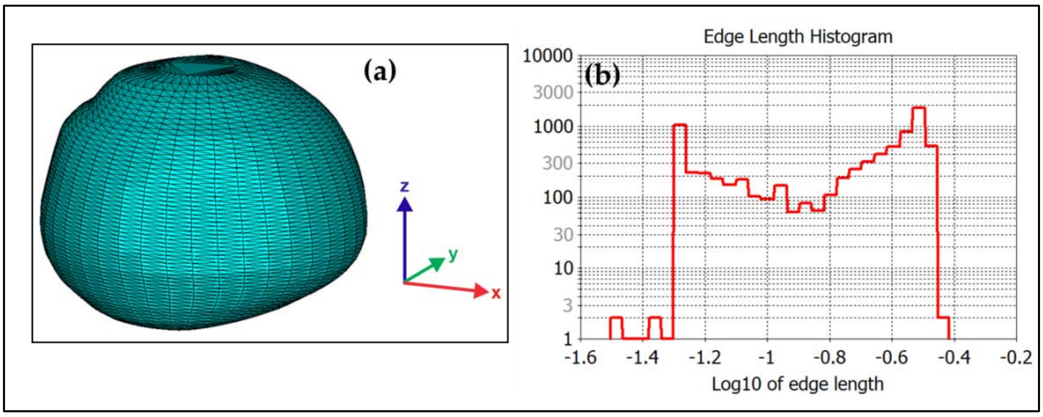

Figure 3. (a) Triangle mesh of an individual drop imported into CST Microwave Studio; **(b)** histogram of the edge length of the triangulation

A plane wave excitation source was defined with linear polarization and a frequency of 5.625 GHz. The Radar Cross Section (RCS) of each individual drop was calculated for both horizontal and vertical polarization using the CST Integral Equation Solver which is suitable for electrically large dielectric objects. Results are presented in the next section.

5. Results for individual particles

RCS calculations were carried out for 0° to 359° angles with 1° step size, in order to cover all possible look angles in the horizontal plane. To ensure plausibility of the results, the calculated RCS of all 601 individual drops were compared to the respective values of equal volume spheres. Figure 4 illustrates the RCS in terms of the equi-volume drop diameter for one defined view angle in panel (a) as well as for the averaged RCS over all orientations within 360° in panel (b). The figures show that the modelled shape can differ by ± 3 dB from a sphere representation.

Panel (c) shows the same points as panel (b) for H and V polarizations for all look angles, but here we have superimposed two curves which represent the RCS variation when a fixed shape-size relationship is used, in this case, the oblate-spheroid approximation of the Beard-Chuang (1984) shapes. The curves are shown as black solid line for H polarization and black dashed line as V polarization. All variations show a general increase in RCS with drop diameter, at least up to 4 mm. Since the shape is fixed for a given drop size, the scattering amplitude will be expected to be a single curve for a given polarization. Furthermore, the rotational symmetry of the drop shape will result in RCS being independent of the look angle. The scatter in the RCS values for the reconstructed drops is of course due to both variation in shapes and the variation with look angle, but even so they appear to lie evenly scattered on both sides of the two (solid black and dashed black) curves.

The differential reflectivity of each reconstructed drop is obtained from the difference between the horizontal and vertical polarization radar cross-sections. Because both the H and V radar cross sections for any given drop will vary with the look angle, its differential reflectivity will also have a φ variation. This has been illustrated in [9] in terms of the complex scattering amplitudes for both polarizations (see their Fig. 7 where φ was varied from 0 to 360 deg in the horizontal plane).

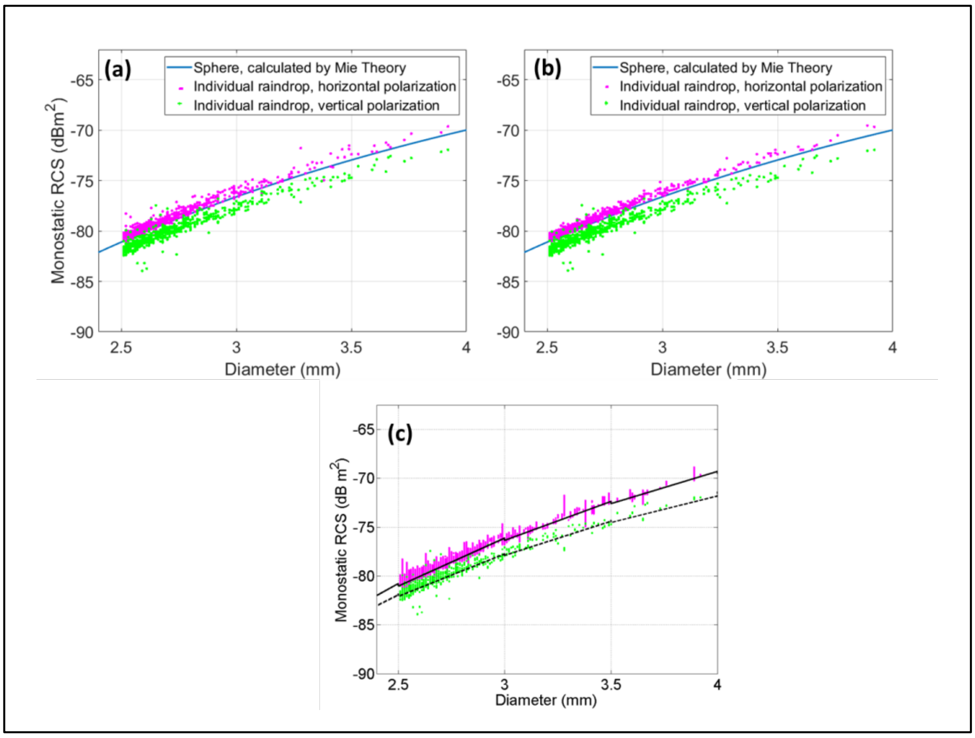

Figure 4. Radar Cross Section (RCS) of 601 reconstructed raindrops for horizontal and vertical polarization, as a function of their respective equal volume diameter. For comparison, the RCS of a sphere is shown. f = 5.625 GHz and the refractive index m = 8.6137 - j1.3020. Panel (a) is for a fixed view angle of φ = 0 and panel (b) is the averaged value of the RCS over φ = 0 to 359°. Panel (c) shows the same RCS versus D_{eq} as panel (b) for the reconstructed drops for H and V polarizations, compared with those assuming Beard-Chuang shapes.

The overall variation of Z_{dr} with drop diameter for all the 601 drops is shown in panel (a) of Fig. 5 as cyan color points. For comparison, the theoretical curve assuming the Beard-Chuang drop shape model [1] (approximated to oblate spheroids) is included as blue dotted line. The zoomed in version for D_{eq} up to 4 mm is shown in panel (b) for more clarity. In both cases, the cyan points cover the full range of φ from 0 to 360 (or 180) degrees. Superimposed on the plots are red points which correspond to φ=50 deg, which in fact is close to the look angle (i.e. azimuth) from the ARMOR radar site to the 2DVD location.

From Fig. 5, certain observations can be made:

(i) Compared to the theoretical curve, Z_{dr} values for individual drops can differ by several dB's, indicating considerable amount of shape deviations from the 'equilibrium' shapes.
(ii) However majority of the deviations span both positive and negative values, implying the drop shapes can be 'elongated' either in the horizontal plane or along the vertical, due to drop oscillations (including mixed-mode).
(iii) The φ=50 deg points show less scatter than the φ = 0 to 360 deg (cyan) points; this is to be expected.
(iv) The resonance region around D_{eq} = 6 mm will not have any implications for the Nate storm since all drops recorded were much smaller.

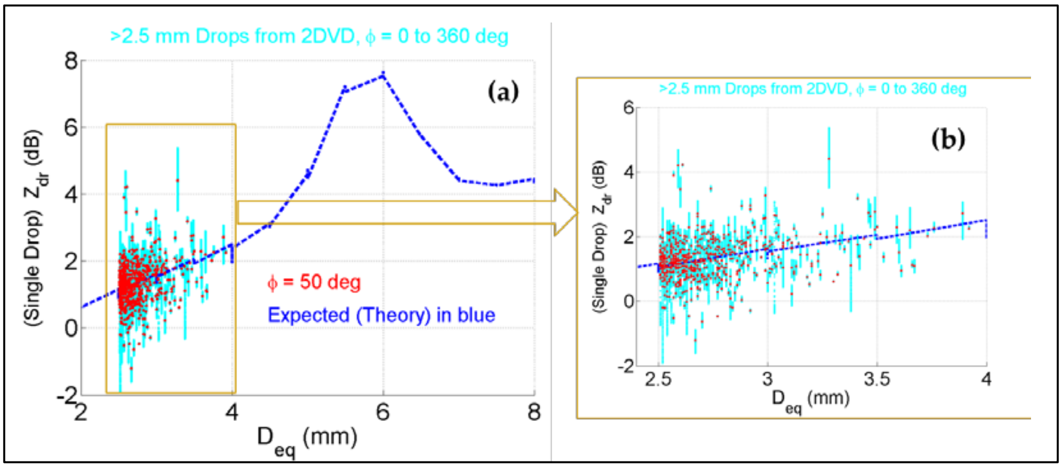

Figure 5. (**a**): Single drop Z_{dr} versus D_{eq} for the reconstructed drops for all φ angles in cyan and for φ=50 deg in red, together with those for a fixed shape-size drop model in blue; (**b**) same as panel (**a**) but zoomed in to cover the brown dotted line box.

The set of panels in Fig. 6 summarizes the drop sizes for the period during which D_{eq} >2.5 mm were recorded as well as the shape deviations quantified in terms of Z_{dr}. Panel (a) shows the drop diameters and panel (b) shows the calculated Z_{dr} in red for each drop and the theoretical (expected) value in blue, as well as the difference $\delta(Z_{dr})$ between the two in magenta. Panels (c) and (d) show the variation of $\delta(Z_{dr})$ with D_{eq} and the expected Z_{dr} respectively. Note panels (b), (c) and (d) correspond to φ=50 deg.

Once again, we summarize the important observations: (i) that TS Nate did not produce drops larger than 4 mm over Huntsville (as mentioned earlier); (ii) $\delta(Z_{dr})$ can be significant but overall they tend to be distributed evenly around the 0 dB level, although the larger drops (> 3 mm) $\delta(Z_{dr})$ shows tendency to be slightly more negative, i.e. drops being somewhat closer to spherical in shape; (iii) that the skewness towards negative $\delta(Z_{dr})$ values are more apparent at around just prior to 15:00 UTC when the wind speeds are seen to increase and the change in wind direction is more rapid. It is around this time, that the fall velocities also show a small but noticeable number of drops having lower than expected velocities. This may provide further evidence that turbulence may contribute toward enhanced amplitude of mixed mode oscillations, as was observed in two earlier studies, one during category-1 hurricane Irma, and the other during a highly organized line convection [23], [11].

 doi:10.20944/preprints201910.0284.v1

Peer-reviewed version available at Atmosphere 2020, 11, 114; doi:10.3390/atmos11010114

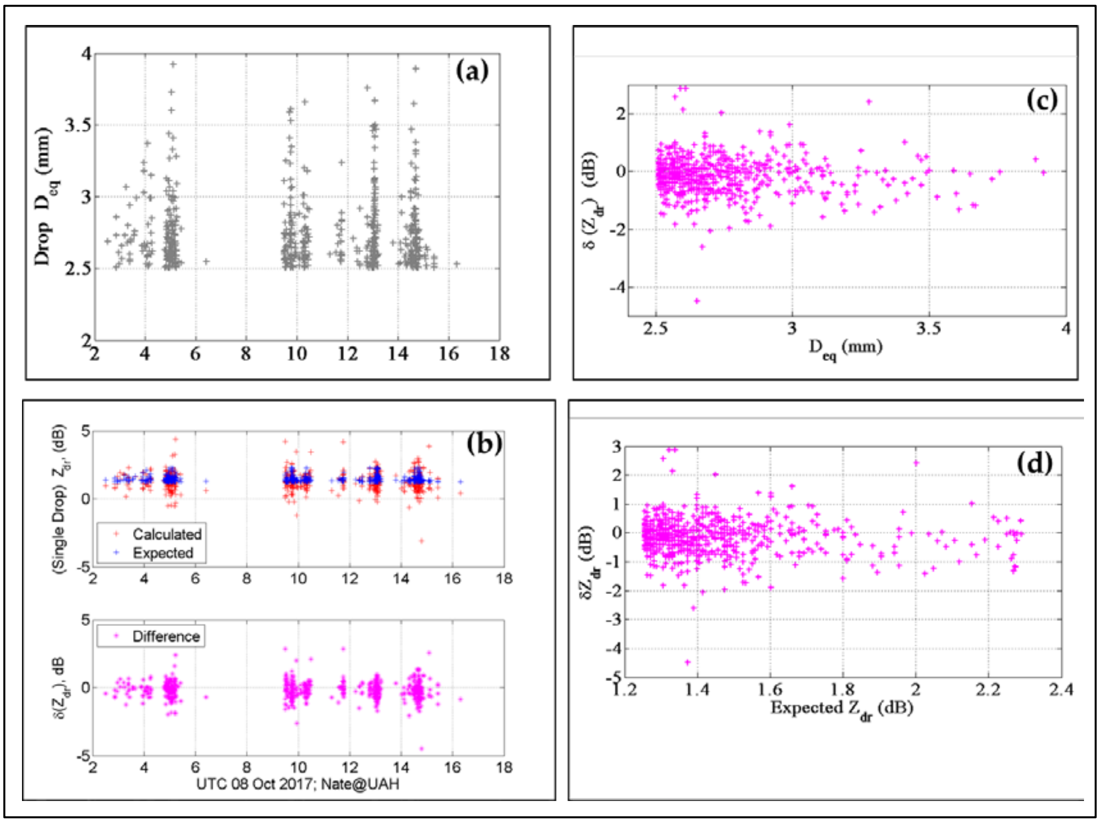

Figure 6. (**a**) Diameters of all drops > 2.5 mm recorded during the passage of TS Nate over the 2DVD; (**b**) the calculated Z_{dr} for each drop in red and the expected value in blue (top plot) and the difference in Z_{dr}, δZ(dr), for each particle; (**c**) δ(Z_{dr}) versus D_{eq}; (**d**) δZdr versus the expected Z_{dr}.

The vertically pointing X-band Doppler radar shows evidence of moderate convection at around 14:40 UTC compared with other time periods. Fig. 7 is an expanded plot of the Z-height profile measurements for a 1-hour period from 14:00 to 15:00 UTC. The marked period shows more clearly the moderate convection near the melting layer of around 4.8 km, which in fact corresponds to the outer-band shown earlier from the radar-mosaic image in Fig. 1. To be more precise, the 'more diffused bright-band' in terms of Z and Doppler mean velocity associated with the outer-band is seen at 14:35 UTC at the melting layer height whereas significant δ(Z_{dr}) was obtained at around 14:42 UTC at ground level, with δ(Z_{dr}) tending to be more negative and the fall velocities tending to be somewhat lower than the expected values. The time difference accounts for the drops to fall from the bottom of the melting level to ground level.

The extent of the negative δ(Z_{dr}) for > 2.5 mm drops can be seen in panel (a) of Fig. 8 which shows the overall histogram. The mode of the distribution lies very close to 0 dB however significantly more negative δ(Z_{dr}) are observed, compared with positive δ(Z_{dr}). To quantify this, as an example, 149 drops out of 601 drops had δ(Z_{dr}) less than -0.5 dB whereas only 72 drops had δ(Z_{dr}) greater than 0.5 dB. By way of comparison, panel (b) shows the δ(Z_{dr}) histogram derived from the 80 m fall artificial rain experiment [3], where only 5% of the measured drops were found to have significant asymmetry. Here, the axis ratios have been used to convert to δ(Z_{dr}) values using the expression from [24]:

$$10^{-0.1(Z_{dr})} = \left(\frac{a}{b}\right)^{\frac{7}{3}} \qquad (1)$$

The distribution of δ(Z_{dr}) in panel (b) is visibly more symmetric than panel (a), although the extent of the distribution is slightly wider than panel (a).

Preprints (www.preprints.org) | NOT PEER-REVIEWED | Posted: 25 October 2019 doi:10.20944/preprints201910.0284.v1

Peer-reviewed version available at Atmosphere 2020, 11, 114; doi:10.3390/atmos11010114

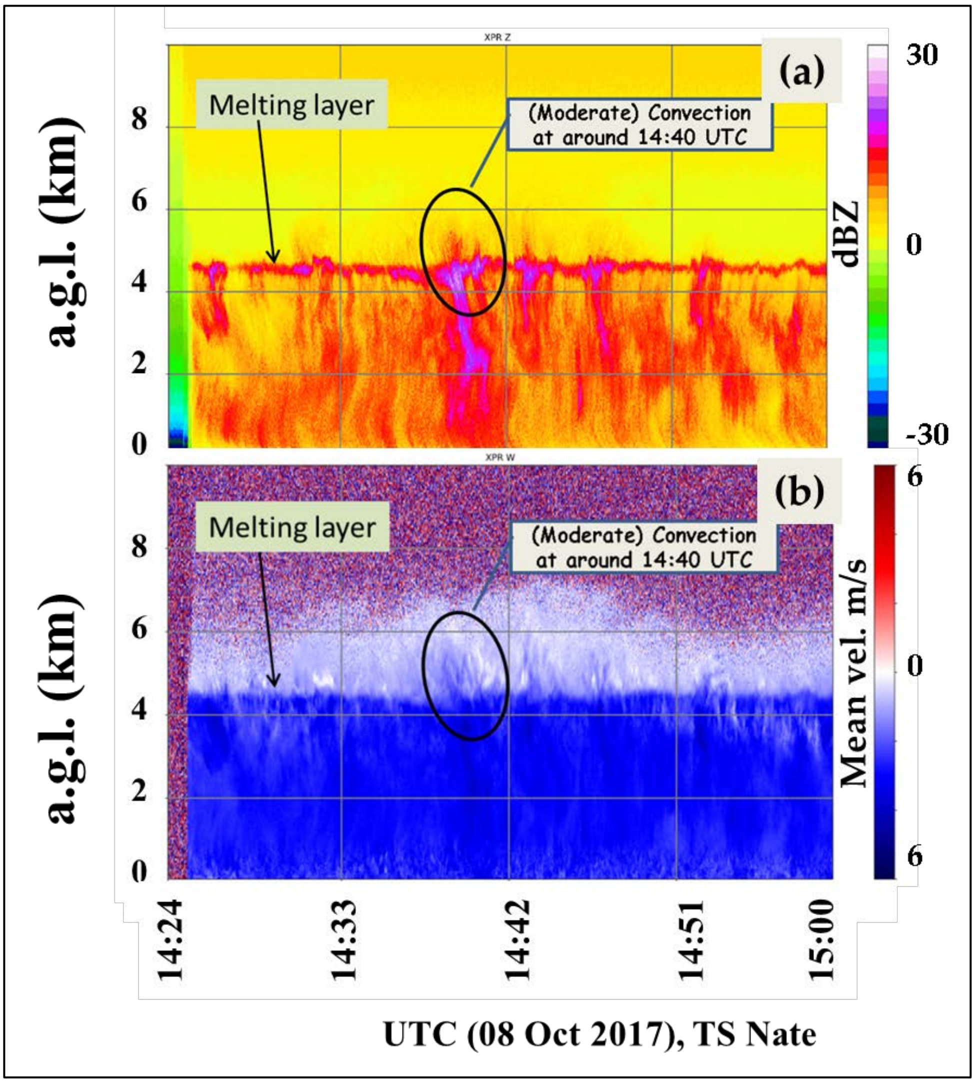

Figure 7. (**a**) Vertical profiles of dBZ from the vertically-pointing XPR observations for 14:24 to 15:00 UTC on 08 Oct 2017; (**b**) the corresponding Doppler mean velocity. Courtesy of K. Knupp of University of Alabama, Huntsville.

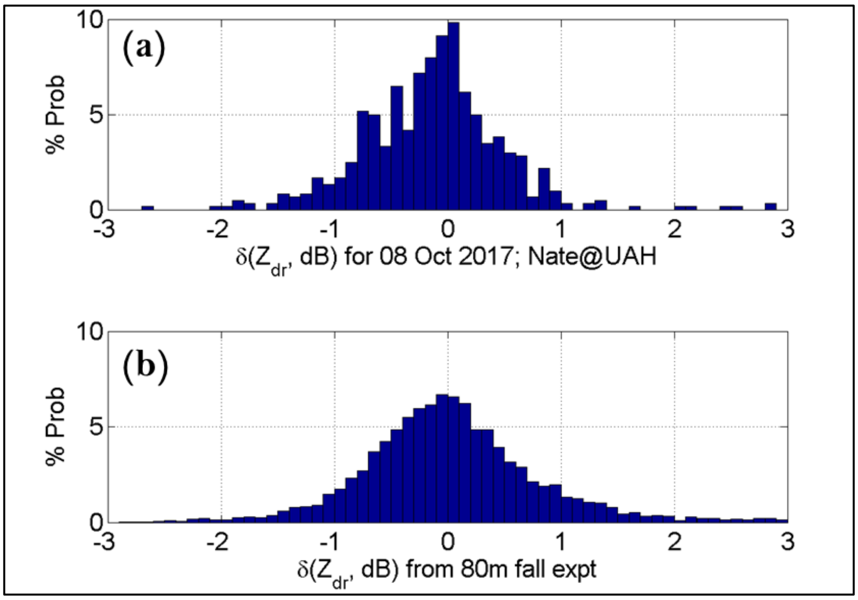

Figure 8. Histograms of $\delta(Z_{dr})$ for all > 2.5 mm drops (**a**) for the reconstructed drops during TS Nate and (**b**) for drops recorded during the 80 m fall experiment [4] using eq. (1).

Preprints (www.preprints.org) | NOT PEER-REVIEWED | Posted: 25 October 2019 doi:10.20944/preprints201910.0284.v1

Peer-reviewed version available at Atmosphere 2020, 11, 114; doi:10.3390/atmos11010114

6. 1-minute based Z_h, Z_{dr} calculations and comparisons with ARMOR

To compute the overall back scatter reflectivity from the individual scattering amplitudes, for example over a 1-minute period, we perform drop-by-drop integration of the radar cross-sections (strictly speaking the covariance matrix elements) during that time period. If we denote the H-polarization reflectivity for the i^{th} drop as z_i^h, then the overall reflectivity from all drops over the 1-minute period is given by:

$$Z_h = \frac{1}{A\Delta t} \sum_{i=1}^{n} v_i^{-1} z_i^h \qquad (2)$$

where A is the measurement area of the 2DVD, Δt is the averaging time period, and v_i is the vertical velocity of the ith drop. For V polarization, similar integration is performed using the corresponding RCS values, z_i^v. Both are converted to the conventional dBZ units and Z_{dr} for that 1-minute period is determined from the difference between the two.

The 1-minute based calculations for the entire 18 hour event period is shown in Fig. 9 and compared with the C-band ARMOR radar data over and in the vicinity of the disdrometer site. Panel (a) shows the Z comparison, and panel (b) the Z_{dr} comparison. After 05:00, there is excellent agreement in both cases. Some smoothing has been applied to both sets of plots in order to reduce the noise and show more clearly the close agreement. Prior to 05 hr UTC, radar Z appears to be somewhat lower than the simulations and the Z_{dr} slightly higher. It was around this time that the retrieved horizontal drop velocities (from 2DVD measurements) showed some discrepancy with the wind sensor data. Hence it is possible that the shape reconstruction is not precise enough to provide sufficiently accurate scattering amplitudes. On the other hand, the radar data shows highly fluctuating Z_{dr} at the beginning of the storm, so that too may have contributed to the discrepancy.

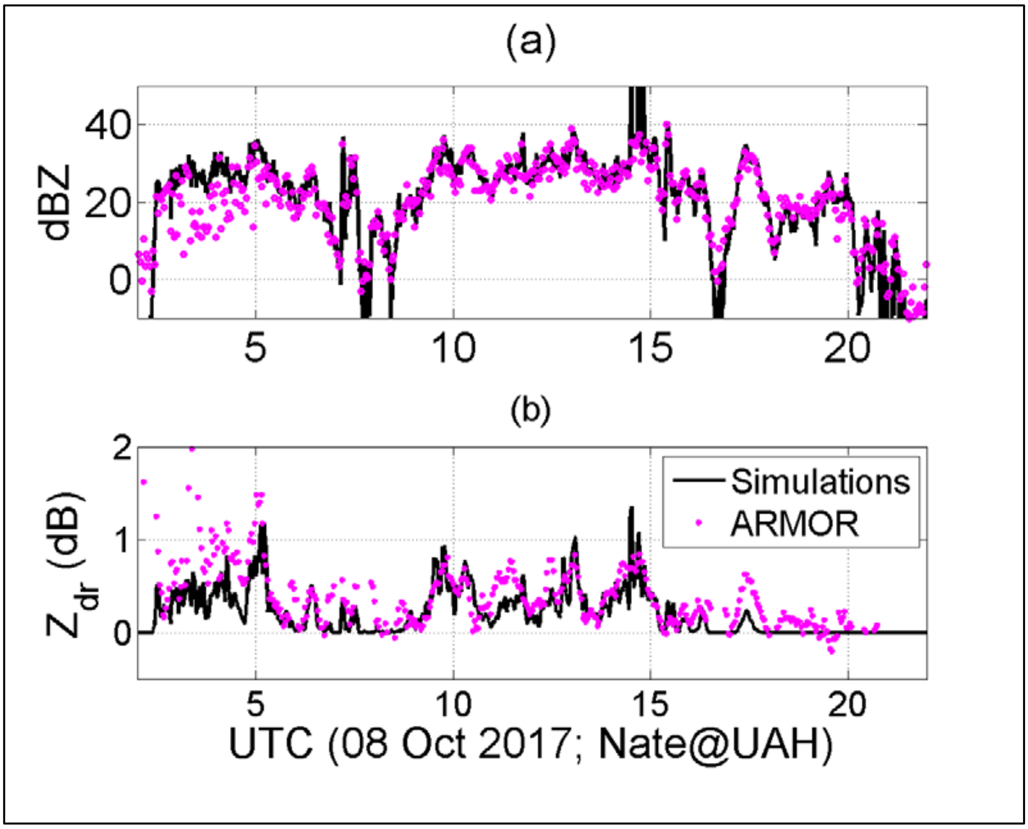

Figure 9. (**a**) dBZ and (**b**) Z_{dr} calculations derived from the individual drop scattering amplitudes using the 2DVD measurements (in black) compared with the ARMOR radar measurements (majenta) over the 2DVD site. For the former, 1-minute time interval is used.

Preprints (www.preprints.org) | NOT PEER-REVIEWED | Posted: 25 October 2019 doi:10.20944/preprints201910.0284.v1

Peer-reviewed version available at *Atmosphere* **2020**, *11*, 114; doi:10.3390/atmos11010114

The Z_{dr} versus Z_h variation from the CST simulations for 05-20 hr UTC are compared with those from the radar observations in Fig. 10. The variations are in good agreement with each other and both show a clear increase of Z_{dr} with increasing Z_h beyond 22 dBZ. Note also the maximum reflectivity values for both cases did not go beyond 40 dBZ and the maximum Z_{dr} did not go beyond 1.5 dB. All these features provide confirmation and validation for the drop-by-drop based scattering calculations.

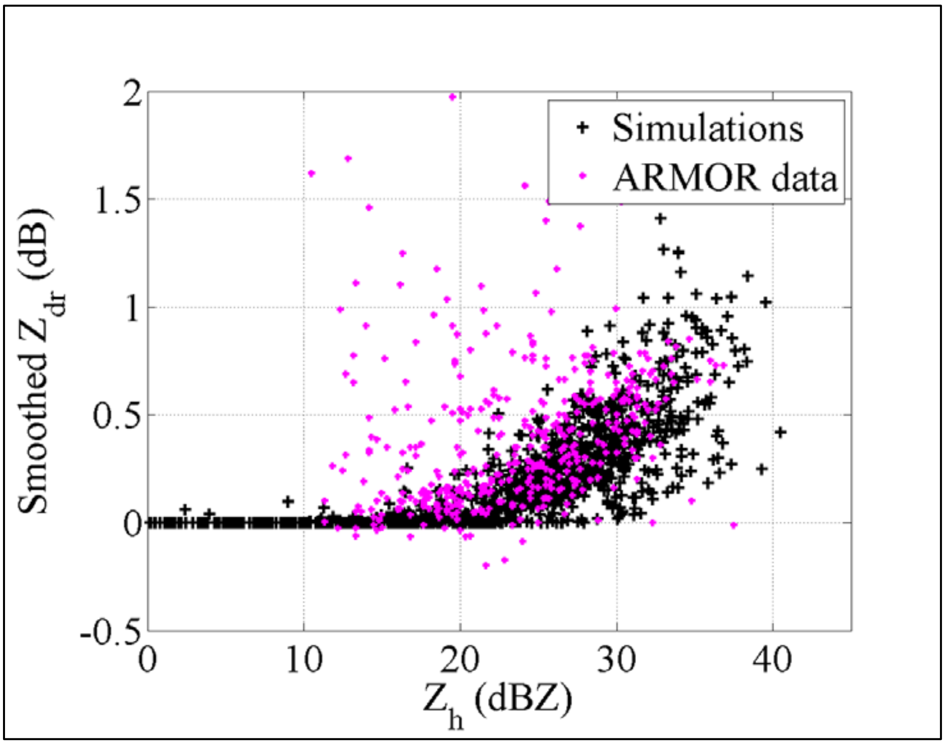

Figure 10. Z versus Z_{dr} corresponding to Fig. 9.

7. Discussion and Conclusions

Thus far the analyses of the 2DVD measurements during the Nate storm over Huntsville and the scattering calculations have provided the following observations and highlights:

(i) Confirmation that horizontal velocity of the drops is very similar to the wind velocities, both in terms of magnitude and direction;
(ii) Fall velocities largely follow the Atlas et al. [21] variation with drop diameter for this event, although some scatter is evident, particularly during the (modest) convection period.
(iii) Shape deviations from the most probable shapes can be significant, as can be inferred from their scattering amplitudes for horizontal and vertical polarizations for individual drops compared with equilibrium-shaped drops,
(iv) Additionally, and as a result, the differences in the calculated Z_{dr} and the expected Z_{dr} show a histogram with a relatively broad distribution,
(v) Overall however the histogram of the differences have a mode at 0 dB, although some skewness towards negative values is indicated, implying some tendency towards more spherical-like drops.
(vi) The Z and Z_{dr} calculated using the individual C-band scattering amplitudes of each drop over say 1-minute interval shows, in general, excellent agreement with the C-band radar observations over the disdrometer for the entire 18 hour period of TS Nate in Huntsville.

Regarding (i), even though it is well known from theory that horizontal velocities of precipitation particles will be the same as the prevalent wind velocities (e.g. [25], [26]) during steady conditions, it is only the 2DVD instrument which is capable of providing direct observational evidence on a drop-by-drop basis in natural rain. Examples have been demonstrated in previous studies ([9], [23]) for a line convection event and a hurricane event which showed excellent agreement of the 2DVD-based drop horizontal velocities at near-ground level with the wind measurements at 10 m height. Such agreement has also been observed for several other events also (not published). Altogether they categorically show (a) that there is very little difference in wind speeds between 10 m height and near ground level, and (b) that the instrument itself (the low-profile design) does not cause any perturbations in the local wind conditions.

Along the vertical, the drop fall velocities (point (ii) above) show a distribution of velocities which are mostly Gaussian-shaped, with a mean and mode very close to that predicted by the Atlas et al. [21] equation. During the (moderate) convection period, the fall velocities showed somewhat more scatter than at other times. However there were no time periods where there was noticeably negative bias (i.e. slowing down of the drops). This is in contrast to the hurricane (category-1) Irma event which had lower than expected velocities during turbulence , as well an embedded line convection period where low fall speeds were associated with a rapid change in wind direction (see [23] for both cases). Such changes were not observed with the anemometer readings during TS Nate at Huntsville. In general, the fall velocities (at least for > 2 mm) tend to follow the Atlas et al. 1973 equation except for events associated with high turbulence. Another example is Tropical Storm Michael which had passed over another 2DVD instrument (unit number SN70) located at Wallops flight facility in Virginia, USA. This storm had high wind gusts associated with it, and the 2DVD-SN70 measurements clearly had shown significant reduction in fall speeds for drops within the leading eye-wall region of the storm (see Appendix). In other parts of the storm, fall velocities were close to the expected values. This too should be considered as evidence for reduced fall speeds being associated as a response to turbulence. The observations are in agreement with the theoretical work by Stout et al. [27] who simulated the motion of drops in isotropic turbulence to show that there would be a reduction (> 35%) of the average drop settling velocity, relative to terminal velocity, for larger drops with inertia (> 2 mm). This is largely due to a net upward component of the non-linear drag forces generated under turbulent conditions. Note there are also other factors which can affect drop terminal velocities; for example Gay et al. [28] have demonstrated the changes in fall velocities can occur for drops falling in strong electric fields.

Regarding point (iii), we have seen from Fig. 4(c) how the scattering amplitudes can be different for the reconstructed drops compared with those using a specific drop shape-size relationship (e.g. from [1]). The differences can be significant for both polarizations, although the two curves for the fixed shape-size variation lie somewhere in the middle of the scatter (of the individual, scattered, points) observed with the reconstructed shapes. The differences occur obviously because of changes in drop shapes which in turn can be attributed to drop oscillations, the amplitudes of which can be expected during significant turbulence. Note also that there could be possible coupling between change in drop shapes and fall velocities [27], [29], [30].

For a given drop equi-volume diameter, variations in drop shape and hence their scattering amplitudes give rise to a distribution of Z_{dr} values. For drops possessing considerable asymmetry, the Z_{dr} will also depend on the look angle. When expressed in terms of $\delta(Z_{dr})$, i.e. the difference from the fixed shape-size variation, the histogram, although showing a wide distribution, has a mode at 0 dB. The histogram does show some skewness towards negative values indicating a tendency towards more spherical shapes, mostly the > 3 mm drops. In general, the scatter in $\delta(Z_{dr})$ is more evident when the wind direction has a more rapid change. This was even more evident in a previously analyzed convection line event (see Fig. 4 in [10] and Fig. A1 in [9]), at the time when the embedded convection line had crossed the 2DVD instrument (between 03:35 to 03:40 UTC on 25 Dec 2009). As mentioned earlier, the larger drops also showed a considerable reduction in fall speeds during the same time interval. For the TS Nate, the convection was at best very moderate which

Preprints (www.preprints.org) | NOT PEER-REVIEWED | Posted: 25 October 2019 doi:10.20944/preprints201910.0284.v1

Peer-reviewed version available at Atmosphere 2020, 11, 114; doi:10.3390/atmos11010114

occurred at around 14:40 to 14:45 UTC (Fig. 7) which is when the most amount of scatter in the calculated single particle $\delta(Z_{dr})$ was observed (along with the highest variation in the fall velocities).

Regarding the final point (iv), the calculated Z_h and Z_{dr} based on the individual scattering amplitudes at C-band over a 1-minute time interval show very close agreement with the radar observations made over the instrument site throughout the entire event. Some minor differences in Z were observed during the beginning of the storm and minor differences in Z_{dr} towards the end of the storm. These could be attributed to non-homogeneity along the vertical (i.e. with height) from the radar pulse-volume to ground level. The calculated Z_{dr} versus Z variation also show excellent agreement with the radar observations.

In terms of the differential backscatter phase, the scattering calculations for the >2.5 mm drops did not show any appreciable differences in the back scatter phase between the H and V polarization implying that resonance scattering does not play a significant role. Consequently the calculated copolar correlation coefficients were close to 1 which is also largely in agreement with radar measurements when reflectivity values exceeded 15 dBZ.

Finally, as a general comment, the following point is worth noting: Strictly speaking, rather than considering drops with a fixed axis ratio-size relationship and a typical canting angle distribution for Z and Z_{dr} calculations (which is often the case), the individual drop-by-drop shape should be used as input for scattering calculations. For the TS Nate event over Huntsville however, T-matrix calculations at C-band using the fixed axis ratio-size assumption did not differ markedly from those using the drop-by-drop scattering amplitudes (not shown here). Several other event analyses have also shown this to be the case. For events with large drops which are associated with high wind speeds and/or rapid change in wind direction (or even high atmospheric e-filed), one may expect a drop in the co-polar correlation coefficient as well as significant backscatter differential phase.

APPENDIX: Drop fall Velocities During Tropical Storm Michael

On 12 October 2018, Tropical Storm Michael, after weakening from hurricane force winds, passed directly over a ground instrumentation site in Wallops, Virginia, which had several collocated sensors. Among them were a 2DVD (unit 70) and all-in-1 weather station. Panel (a) of Fig. A1 shows the variation of the wind-speed from the anemometer with time. Four time periods are marked. The first period (i) is prior to 03 hr UTC when the wind-speeds increase rapidly reaching nearly 25 m/s as the leading edge of the eyewall approached the site from south-east. Note these are much stronger winds than those associated with the outer-bands of TS Nate over Huntsville. The second period (ii) at around 04 hr UTC is when the wind velocity dropped to almost 0 m/s as pressure dropped to 987 mb. This can be considered as the center of the eye of the storm. The third period (iii) is when the winds increased to 20 m/s as the rear side of the eyewall traversed the site and the fourth period (iv) is when cool dry air rushed in as the storm center pulled away after 08 hr UTC.

Panel (b) shows, as an example, the measured fall velocities for all 3 mm drops (±0.15 mm) for the whole storm. They were only detected in and around the eye wall regions, hence only the 00 – 09 hr UTC time interval is shown. During the first period, which corresponds to the leading edge of the eye-wall, considerably lower fall speeds are observed from 02:00 to 03:00 UTC, compared with the Gunn-Kinzer range of values marked as orange dashed lines. 3 mm drops were also detected later on, at around 06:30 to 07:00 UTC, which corresponds to time interval between (iii) and (iv). Here the drops do not show any systematic reduction in fall velocities. The wind speeds at this time were much lower than those during period (i).

Although the drop shapes have not yet been reconstructed for this case, based on the fall velocity measurements, one would expect shape deformation to be significant in the eye-wall region and not in other parts of the storm.

Preprints (www.preprints.org) | NOT PEER-REVIEWED | Posted: 25 October 2019 doi:10.20944/preprints201910.0284.v1

Peer-reviewed version available at Atmosphere 2020, 11, 114; doi:10.3390/atmos11010114

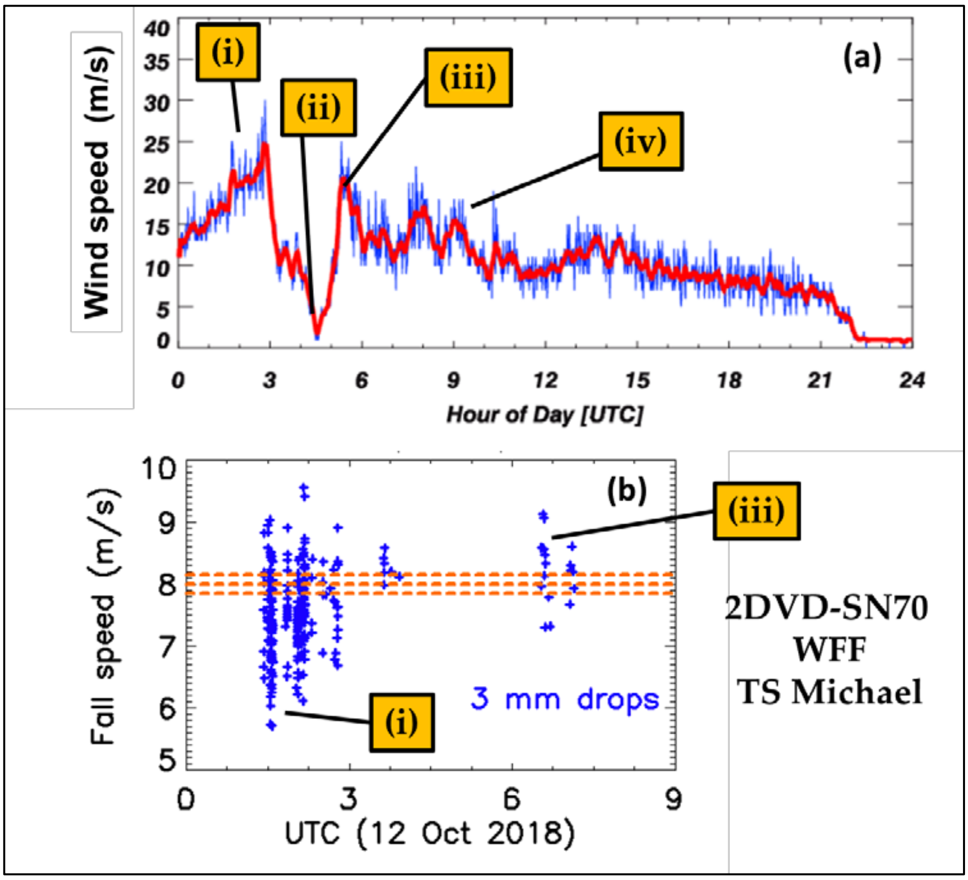

Fig. A1: (**a**) Wind speeds (blue) and averages (red) during TS Michael on 12 October 2018; (**b**) Measured fall velocities for 3±0.15 mm drops. See text for explanation for time periods (i) to (iv). *Panel (a): Courtesy of D. Wolff and D. Marks, NASA-WFF*

Author Contributions: Conceptualization, M.T. and M.S.; Methodology, Investigation and Formal Analysis, S.S., F.T., M.T.; Data Curation, M.T.; Writing-Original Draft Preparation, M.T.; Writing-Review & Editing, F.T., M.S.; Visualization, S.S.; Supervision, F.T.,M.S.; Resources, M.S.

Funding: M.T. received funding to conduct this research from National Science Foundation under Grant AGS-1901585 (PI: V. N. Bringi).

Acknowledgments: We would like to thank Patrick Gatlin and Mathew Wingo for maintaining the 2DVD instruments at the University of Huntsville site and for providing access to anemometer data. Our thanks are also to Prof. Kevin Knupp for providing the XPR data plot used in Fig. 7. Authors would also like to thank David Marks and David Wolff from NASA-Wallops Flight Facility for supplying the 2DVD-SN70 during tropical storm Michael as well as the wind-speed plot in Fig. A1(a). Finally, our thanks to Prof. V.N. Bringi for valueable discussions.

Conflicts of Interest: The authors declare no conflict of interest. The funders had no role in the design of this study; in the collection, analyses, or interpretation of its data; in the writing of this manuscript, and in the decision to publish these results.

References

1. Beard, K.V.; Chuang, C. A new model for the equilibrium shape of raindrops. J. Atmos. Sci., 1987, 44, 1509-1524.
2. Szakáll, M.; Diehl, K.; Mitra, S.K.; Borrmann, S. A wind tunnel study on the shape, oscillation, and internal circulation of large raindrops with sizes between 2.5 and 7.5 mm. J. Atmos. Sci., 2009, 66, 755-765.
3. Thurai, M.; Bringi, V.N. Drop axis ratios from a 2D video disdrometer. J. Atmos. Oceanic Technol., 2005, 22, 966-978.
4. Thurai, M.; Huang, G-J.; Bringi, V.N.; Randeu; W.L.; Schönhuber, M. Drop shapes, model comparisons, and calculations of polarimetric radar parameters in rain. J. Atmos. Oceanic Technol.,2007, 24, 1019-1032.
5. Thurai, M.; Bringi, V.N.; Szakáll, M.; Mitra, S.K.; Beard, K.V.; Borrmann, S. Drop shapes and axis ratio distributions: Comparison between 2D video disdrometer and wind-tunnel measurements. J. Atmos. Oceanic Technol.,2009, 26, 1427–1432.
6. Schönhuber, M.; Schwinzerl, M.; Lammer, G. 3D reconstruction of 2DVD-measured raindrops for precise prediction of propagation parameters. 10th European Conference on Antennas and Propagation (EuCAP), 2016, Davos, Switzerland, IEEE, 3403-3406, https://doi.org/10.1109/EuCAP.2016.7481929.
7. Schwinzerl, M.; Schönhuber, M.; Lammer, G.; Thurai, M. 3D reconstruction of individual raindrops from precise ground-based precipitation measurements. EMS Annual Meeting Abstracts, 2016, Vol. 13, Abstract EMS2016-601, http://meetingorganizer.copernicus.org/EMS2016/EMS2016-601.pdf.
8. Chobanyan, E., N.; Šekeljić, N.; Manic, A.B.; Ilić, M.M.; Bringi, V.N.; Notaroš, B.M. Efficient and accurate computational electromagnetics approach to precipitation particle scattering analysis based on higher-order method of moments integral equation modeling. J. Atmos. Oceanic Technol., 2015, 32, 1745-1758
9. Thurai, M.; Manić, S.B.; Schönhuber, M.; Bringi, V.N.; Notaroš, B.M. Scattering calculations at C-band for asymmetric raindrops reconstructed from 2D video disdrometer measurements. J. Atmos. Oceanic Technol., 2017, 34, 765-776
10. Manić, S.B.; Thurai, M.; Bringi, V.N.; Notaroš, B.M. Scattering Calculations for Asymmetric Raindrops during a Line Convection Event: Comparison with Radar Measurements. J. Atmos. Oceanic Technol., 2018, 35, 1169–1180
11. Thurai, M.; Bringi, V.N.; Petersen, W.A.; Gatlin, P.N. Drop shapes and fall speeds in rain: Two contrasting examples. J. Appl. Meteor. Climatol., 2013, 52, 2567-2581.
12. Schönhuber, M.; Lammer, G.; Randeu, W.L. The 2D-video-disdrometer. Precipitation: Advances in Measurement, Estimation and Prediction, S. C. Michaelides, Ed., 2008, Springer, 3-31.
13. Baumgardner, D.; Kok, G.; Dawson, W.; O'Connor, D.; Newton, R. A new ground-based precipitation spectrometer: The Meteorological Particle Sensor (MPS). 11th Conf. on Cloud Physics, Ogden, UT, Amer. Meteor. Soc., 2002, paper 8.6.
14. Sheppard, B.E.; Joe, P.I. Performance of the precipitation occurrence sensor system as a precipitation gauge. J. Atmos. Ocean. Technol. 2008, 25, 196–212.

Preprints (www.preprints.org) | NOT PEER-REVIEWED | Posted: 25 October 2019 doi:10.20944/preprints201910.0284.v1

Peer-reviewed version available at Atmosphere 2020, 11, 114; doi:10.3390/atmos11010114

15. Hulsey, C.B.; Knupp, K.; An Analysis of a Mesoscale Features during IOP 4C of the VORTEX-SE Field Campaign, 97th American Meteorological Society Annual Meeting, Seattle, WA, January 22-26, 2017.
16. Petersen, W. A.; Knupp, K. R.; Cecil, D. J.; Mecikalski, J. R. The University of Alabama Huntsville THOR Center instrumentation: Research and operational collaboration. 33rd Int. Conf. on Radar Meteorology, Cairns, Queensland, Australia, Amer. Meteor. Soc., 2007, paper 5.1, https://ams.confex.com/ams/33Radar/webprogram/Paper123410.html.
17. Mecikalski, R.M.; Bain, A.L.; Carey, L.D. Radar and Lightning Observations of Deep Moist Convection across Northern Alabama during DC3: 21 May 2012. Mon. Wea. Rev., 2015, 143, 2774-2794
18. Schönhuber, M.; Randeu, W. L.; Urban, H. E.; Poiares Baptista, J. P. V. Field measurements of raindrop orientation angles. Proc. AP2000 Millennium Conf. on Antennas and Propagation, Davos, Switzerland, 2000, IEE, CD-ROM.
19. Gimpl, J. Optimised algorithms for 2d-video-distrometer data analysis and interpretation. Diploma thesis, Institute of Communications and Wave Propagation, Graz University of Technology, Austria, 2003, 111 pp.
20. Gunn, R.; Kinzer, G.D. The terminal velocity of fall for water droplets in stagnant air, J. Meteorol., 1949, 6, 243-248
21. Atlas, D.; Srivastava, R.C.; Sekhon, R.S. Doppler radar characteristics of precipitation at vertical incidence. Rev. Geophys., 1973, 11, 1-35.
22. Ray, P. Broadband complex refractive indices of ice and water. Appl. Opt., 1972, 11, 1836-1844.
23. Thurai, M.; Schönhuber, M.; Lammer, G.; Bringi, V.N. Raindrop shapes and fall velocities in "turbulent times", Adv. Sci. Res., 2019, 16, 95-101, 2019, https://doi.org/10.5194/asr-16-95-2019
24. Jameson, A.R. Microphysical interpretation of multiparameter radarmeasurements in rain. Part I: Interpretation of polarization measure-ments and estimation of raindrop shapes,"J. Atmos. Sci., 1983, 40, 1792-1802.
25. Marshall, J.S. Precipitation trajectories and patterns.J. Meteor., 1953, 10, 25–29.
26. Dawson, D.T.; Mansell, E.R.; Kumjian, M.R. Does Wind Shear Cause Hydrometeor Size Sorting?. J. Atmos. Sci., 2015, 72, 340–348.
27. Stout, J.E.; Arya, S.P.; and Genikhovich, E. L. The effect of nonlinear drag on the motion and settling velocity of heavy particles, J. Atmos. Sci., 1995, 52, 3836-3848
28. Gay, M. J.; Griffiths, R.F.; Latham, J.; Saunders, C.P.R. The terminal velocities of charged raindrops and cloud droplets falling in strong electric fields, Q. J. R. Meteorol. Soc., 1974, 100, 682-687.
29. Brazier-Smith, P.R. On the shape and fall velocities of raindrops. Quart. J. Roy. Meteor. Soc, 1992, 118, 749-766.
30. Coquillat, S.; Combal, B.; Chauzy, S. Corona emission from raindrops in strong electric fields as a possible discharge initiation: comparison between horizontal and vertical field configurations, J. Geophys. Res., 2003, 108 (D7), 4205.